Integrated Experimental-statistical-numerical Framework for Durability and Fracture Performance of Reactive Powder Concrete under Marine Exposure

Mounira CHADLI [1], Kheira Camellia NEHAR [2] *, Dalila BENAMARA [2]

[1] *Civil Engineering Research Laboratory, Department of Civil Engineering and Hydrology, University of Biskra, BP 145RP, Biskra 07000, Algeria*
[2] *Laboratory of Mechanics and Materials Development, University of Djelfa, POBox 3117, 17000 Djelfa, Algeria*

http://doi.org/10.5755/j02.ms.44216

Received 2 February 2026; accepted 24 March 2026

Reactive Powder Concrete (RPC) is an ultra-dense cementitious material whose durability and cracking behavior in aggressive environments are governed by complex physicochemical mechanisms. This study proposes an integrated experimental-statistical-numerical approach to evaluate the durability of RPC subjected to real marine exposure for 12 months. Response Surface Methodology (RSM) combined with Central Composite Design (CCD) was used to optimize key formulation parameters: cement content, silica fume dosage, superplasticizer dosage, water-to-binder ratio, and fiber volume fraction. Compressive strength and microstructural evolution were evaluated experimentally, while Finite Element Method (FEM) and Extended Finite Element Method (X-FEM) simulations were used to model crack initiation and propagation. Experimental tests showed that optimized RPC mixtures retained high compressive strength with minimal cracking under marine exposure. FEM/XFEM simulations predicted crack initiation and propagation, confirming the effectiveness of fiber reinforcement in reducing crack growth. Statistical analysis highlighted cement content and matrix densification as the most influential factors. This approach provides a comprehensive framework for designing durable RPC formulations for marine environments.

Keywords: reactive powder concrete, marine exposure, response surface methodology, modeling, durability, microstructure.

1. INTRODUCTION

Reactive powder concrete (RPC) is an ultra-dense cementitious composite whose performance is determined by a tightly controlled microstructure and complex physicochemical interactions that happen during hydration and long-term exposure [1, 2]. RPC can be viewed as a multi-phase reactive system in which binder composition, particle packing, water-to-binder ratio, and admixture chemistry collectively control hydration kinetics, pore structure refinement, and transport properties [3]. These coupled mechanisms ultimately dictate mechanical performance and durability, particularly in aggressive environments [4].

Marine exposure represents one of the most severe service conditions for cement-based materials due to the combined presence of chloride, sulfate, and magnesium ions [5, 6]. These species interact with hydration products, modifying phase assemblages, destabilizing portlandite, and promoting the formation of secondary products such as gypsum and ettringite [7, 8]. Such chemical transformations alter pore connectivity and mechanical integrity, accelerating degradation processes that cannot be adequately described by compressive strength alone [9]. Consequently, durability assessment of RPC in marine environments requires an integrated approach combining mechanical testing, microstructural characterization, and predictive modeling [10].

Recent studies on RPC and high-performance concretes have predominantly focused on short-term mechanical performance or isolated durability indicators [11]. However, the combined influence of mixture design parameters such as silica fume content, fiber volume fraction, water-to-binder ratio, and superplasticizer dosage on long-term durability and cracking behavior under real marine exposure remains insufficiently understood [12]. From a process optimization standpoint, this knowledge gap limits the rational design of durable cementitious materials for aggressive environments [13].

In this context, statistical design tools such as Response Surface Methodology (RSM) provide an efficient framework for quantifying both individual and interaction effects among formulation parameters while minimizing experimental effort [14]. When coupled with microstructural analysis techniques (XRD and SEM) and numerical modeling approaches such as the Finite Element Method (FEM) and Extended Finite Element Method (X-FEM), RSM enables the development of predictive models linking composition, microstructure evolution, and mechanical response [15].

Accordingly, the present study adopts an integrated experimental-statistical-numerical approach to investigate the durability and cracking behavior of RPC subjected to long-term marine exposure. Optimized RPC formulations are developed using a Central Composite Design, their mechanical performance and microstructural evolution are experimentally characterized after 12 months of seawater immersion, and their cracking behavior is simulated using

* Corresponding author: K.C. Nehar
E-mail: *c.nehar@univ-djelfa.dz*

FEM/X-FEM. This combined methodology provides a robust framework for understanding and predicting the chemo-mechanical behavior of RPC in marine environments, contributing to the design of durable cementitious materials.

2. MATERIALS AND METHODS

2.1. Materials

Ordinary Portland cement (CEM I 42.5 N HRS) supplied from the Enfidha cement plant (Tunisia) was used as the primary binder. Its Blaine fineness and density were 3714 cm²/g and 3.02 g/cm³, respectively. Granulated blast-furnace slag (GS) from the El-Hadjar steel complex (Algeria) exhibited a specific surface area of 7277 cm²/g and a density of 2.60 g/cm³. Crushed quartz powder (CQ), with particle sizes ranging from 10 to 15 µm, had a specific surface area of 5714 cm²/g and a density of 2.63 g/cm³. Silica fume (SF, Condensil S95 DP, Sika) had a density of 1.56 g/cm³. The detailed chemical compositions of all cementitious materials are summarized in Table 1.

Table 1. Chemical compositions of cement, silica fume, slag, and quartz powder in percentage

Cementitious materials	SiO_2	Al_2O_3	Fe_2O_3	CaO	MgO
Cement	20.62	5.31	4.94	64.24	2.01
Silica fume	94.60	1	1	0.40	1
Slag	35.88	14.38	0.56	30.96	8.13
Quartz	94.33	1.171	1.044	1.622	0.184

Fine dune sand (FS) with a maximum particle size of 600 µm was collected from the Djamaa region (Algeria). Its fineness modulus, sand equivalent, and specific gravity were 1.98, 74.9 %, and 2.626 g/cm³, respectively. A polycarboxylate-based superplasticizer (Sika ViscoCrete Tempo 12, density 1.06 g/cm³) was used to ensure adequate workability at low water-to-binder ratios. Hooked steel fibers (Sika RL-45/50-BN) were incorporated to enhance crack resistance. Tap water conforming to NF P 18-404 [16] was used for mixing and curing. The chemical composition of seawater was determined at the Hydraulics Laboratory of the University of Biskra in Algeria (Table 2).

Table 2. Chemical composition of seawater

Composants	PO_4^{-3}, mg/l	SO_4^{-2}, mg/l	NO_2^-, mg/l	NH_4^+, mg/l	Mn^{+2}, mg/l	Fe^{+2}, mg/l	pH
	0.1	0.0282	0.15	3	19.3	0.25	8.38

2.2. Mixtures and mixing procedure

RPC mixtures were designed based on formulations reported in the literature, with a reference water-to-binder ratio close to 0.20 and fiber contents up to 2 % by volume. Cement was partially replaced by slag (15 %) and silica fume (23 – 25 %) to improve long-term performance. The detailed mixture proportions are reported in Table 3.

Dry constituents (sand, cement, quartz powder, slag, and silica fume) were first mixed for 2 min. Water and superplasticizer were then added and mixed for approximately 5 min until a homogeneous paste was obtained. Steel fibers were subsequently introduced and mixed for an additional 3 – 6 min to ensure uniform dispersion. Specimens were cast in molds, cured for 24 h at 20 °C and 95 % relative humidity, and then stored either in potable water or seawater at 20 °C until testing.

2.3. Test methods and procedures

2.3.1. Seawater exposure and mechanical testing

After demolding, specimens were immersed in potable water or seawater at 20 °C for up to 12 months. Workability was assessed using the slump test (NF EN 12350-2). Compressive strength was measured at 365 days on prismatic specimens (40 × 40 × 160 mm³) according to NF EN 12390-4, using the average of three tests.

2.3.2. Microstructural characterization

Microstructural analyses were conducted on powdered fragments collected after compressive testing. X-ray diffraction (XRD) was performed using a Bruker D8 ADVANCE powder X-ray diffractometer equipped with a Cu anode using Cu Kα radiation, at the laboratory of the University of Biskra (Algeria), and phase identification was carried out with X'Pert HighScore software. Scanning electron microscopy (SEM) observations were performed using an SE detector at an accelerating voltage of 20 kV.

2.4. Statistical design and numerical modeling

2.4.1. Statistical part

A CCD within the RSM framework was employed to evaluate the effects of cement content (C), silica fume dosage (SF/C), superplasticizer dosage (SP/C), water-to-binder ratio (W/B), and fiber volume fraction (FM) on compressive strength.

2.4.2. Modeling study

Numerical simulations were performed using the FEM to reproduce the mechanical response of RPC specimens, while crack initiation and propagation were analyzed using the X-FEM. Material parameters were derived directly from experimental results to ensure consistency between experimental and numerical analyses.

Table 3. Composition of concrete

	C, kg/m³	FS/C	SF/C	CQ/C	GS/C	SP/C	W/B	FM, %
RPCC	975	1.1	0.23	0.23	0.15	0.027	0.23	0
RPCF1	950	1.1	0.25	0.23	0.15	0.020	0.27	2
RPCF2	955	1.1	0.23	0.23	-	0.050	0.20	2
RPCF3	930	1.1	0.25	-	0.15	0.018	0.23	1

3. RESULTS AND DISCUSSION

3.1. Experimental part

The experimental investigation focused on the compressive strength development of RPC mixtures after 12 months of curing in potable water and seawater. Workability was evaluated using the slump test in accordance with NF EN 12350-2, while compressive strength was measured on prismatic specimens (40 × 40 × 160 mm³) following NF EN 12390-4.

Fig. 1 and Fig. 2 present the evolution of compressive strength for the different RPC formulations under potable water and seawater exposure.

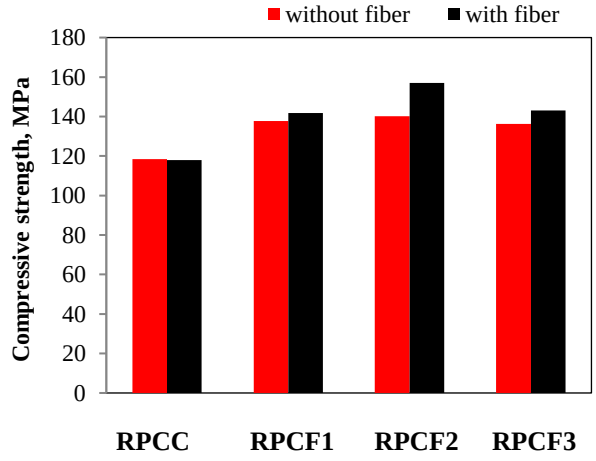

Fig. 1. Compressive strength as a function of immersion time in potable water, after 12 months

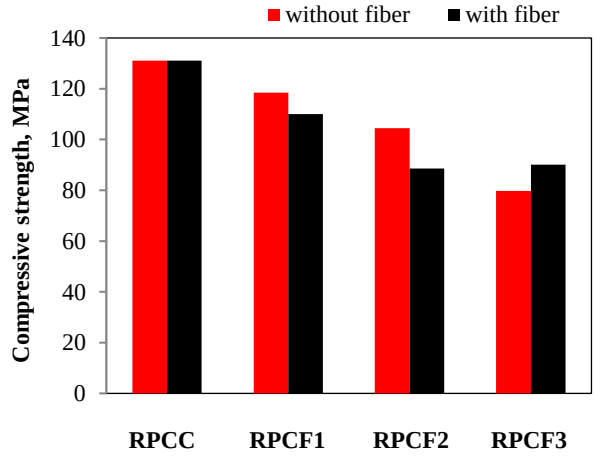

Fig. 2. Compressive strength as a function of immersion time in seawater, after 12 months

After 12 months, fiber-free mixtures stored in seawater exhibited higher compressive strength than some fiber-reinforced counterparts, whereas a general reduction in strength was observed for fiber-containing mixtures, particularly RPCF1. This reduction can be attributed to chemical interactions with chloride- and carbonate-rich seawater, which promote carbonation and destabilization of portlandite, in agreement with previous findings [17, 18].

The incorporation of ground granulated slag resulted in lower early compressive strength compared to slag-free formulations, while silica fume significantly enhanced strength due to its pozzolanic activity and pore refinement effect. Mixtures incorporating 15 % slag and approximately 25 % silica fume achieved compressive strength values exceeding 130 MPa after 365 days, consistent with observations reported in the literature [19].

In most cases, specimens cured in potable water exhibited higher compressive strength than those exposed to seawater, highlighting the deleterious effect of the marine environment on long-term mechanical performance. Nevertheless, the results demonstrate that appropriate optimization of binder composition can effectively mitigate strength loss under aggressive marine conditions.

This strength reduction under seawater exposure is primarily attributed to chemically driven alterations of the hydration products, including partial portlandite destabilization and the formation of secondary saline phases, which locally modify the pore structure and stress distribution within the cementitious matrix.

3.2. Statistical part

In the second phase of this study, a Central Composite Design (CCD) within the Response Surface Methodology (RSM) framework was used to evaluate the influence of mixture parameters on compressive strength [20]. Five independent variables were considered: cement content (C), silica fume dosage (SF/C), superplasticizer dosage (SP/C), water-to-binder ratio (W/B), and fiber volume fraction (FM), coded as A, B, C, D, E, respectively (Table 4).

The final design matrix consisted of 43 experimental observations after consolidation of replicated center-point measurements (Table 5). Since individual replicate data were not retained separately, the residual variance was treated as a single global error term, and no partition into pure error and lack-of-fit was performed. Model adequacy was therefore assessed using the global F-test, coefficient of determination (R^2), adjusted R^2, predicted R^2, adequate precision, and coefficient of variation.

Second-order polynomial models were fitted to the experimental data for compressive strength in potable water (CSp) and seawater (CSs) [21].

Table 4. Coding and real levels for CCD models

Variables	Unit	Symbol	Coded factor levels				
			-1.68	-1	0	+1	+1.68
Cement (C)	kg/m³	A	930	943.05	952.50	961.96	975
SF/C	/	B	0.23	0.236	0.24	0.244	0.25
SP/C	/	C	0.018	0.0273	0.0340	0.0407	0.050
W/B	/	D	0.20	0.220	0.235	0.250	0.27
FM	%	E	0	0.58	1	1.420	2

Table 5. Experimental results

Mixture	C, kg/m^3	SF/C	SP/C	W/B	FM, %	CSp, MPa	CSs, MPa
1	943.04	0.236	0.027	0.220	0.580	143.9	103.26
2	961.96	0.236	0.027	0.220	0.580	157.01	88.6
3	943.04	0.244	0.027	0.220	0.580	142.58	102.93
4	961.96	0.244	0.027	0.220	0.580	150.51	99.79
5	943.04	0.236	0.041	0.220	0.580	140.44	105.22
6	961.96	0.236	0.041	0.220	0.580	145.81	102.66
7	943.04	0.244	0.041	0.220	0.580	140.57	109.96
8	961.96	0.244	0.041	0.220	0.580	144.96	108.75
9	943.04	0.236	0.027	0.250	0.580	141.58	109.93
10	961.96	0.236	0.027	0.250	0.580	146.51	101.79
11	943.04	0.244	0.027	0.250	0.580	142.42	110.25
12	961.96	0.244	0.027	0.250	0.580	145.2	108.46
13	943.04	0.236	0.041	0.250	0.580	140.57	106.96
14	961.96	0.236	0.041	0.250	0.580	140.96	108.76
15	943.04	0.244	0.041	0.250	0.580	143.86	103.34
16	961.96	0.244	0.041	0.250	0.580	141.17	108.49
17	943.04	0.236	0.027	0.220	1.420	140.58	109.93
18	961.96	0.236	0.027	0.220	1.420	146.51	101.79
19	943.04	0.244	0.027	0.220	1.420	140.43	110.25
20	961.96	0.244	0.027	0.220	1.420	141.2	108.46
21	943.04	0.236	0.041	0.220	1.420	140.57	109.96
22	961.96	0.236	0.041	0.220	1.420	140.96	108.76
23	943.04	0.244	0.041	0.220	1.420	143.86	103.34
24	961.96	0.244	0.041	0.220	1.420	141.17	108.49
25	943.04	0.236	0.027	0.250	1.420	140.42	110.25
26	961.96	0.236	0.027	0.250	1.420	141.19	108.46
27	943.04	0.244	0.027	0.250	1.420	143.43	102.21
28	961.96	0.244	0.027	0.250	1.420	140.94	108.78
29	943.04	0.236	0.041	0.250	1.420	143.86	103.34
30	961.96	0.236	0.041	0.250	1.420	141.17	108.49
31	943.04	0.244	0.041	0.250	1.420	154.12	90.37
32	961.96	0.244	0.041	0.250	1.420	146.44	98.87
33	930	0.240	0.034	0.235	1.000	143.05	90.09
34	975	0.240	0.034	0.235	1.000	140	85
35	952.5	0.230	0.034	0.235	1.000	141.9	110.4
36	952.5	0.250	0.034	0.235	1.000	143.1	111.6
37	952.5	0.240	0.018	0.235	1.000	140.8	108.7
38	952.5	0.240	0.050	0.235	1.000	144.3	112.8
39	952.5	0.240	0.034	0.200	1.000	139.5	106.9
40	952.5	0.240	0.034	0.270	1.000	138.6	105.3
41	952.5	0.240	0.034	0.235	0.000	137.5	116.8
42	952.5	0.240	0.034	0.235	2.000	140.2	107.6
43	952.5	0.240	0.034	0.235	1.000	141.79	110.03

3.2.1. Compressive strength (ANOVA results)

The ANOVA results for compressive strength under potable water exposure (Table 6) indicate that the developed reduced quadratic model is statistically significant ($p < 0.0001$), with an overall model F-value of 5.64. The inclusion of F-values for each term provides a clear quantification of their relative contributions to the response.

While the main effect of cement content (A) is not statistically significant when considered independently, several interaction terms involving cement content (AC, AD, AE, and CE) exhibit strong statistical significance, as reflected by their high F-values and low p-values. This indicates that compressive strength development under potable conditions is primarily governed by interaction effects rather than isolated parameters, highlighting the coupled nature of the underlying physicochemical mechanisms.

The statistical indicators confirm satisfactory model adequacy, with $R^2 = 0.7582$, adjusted $R^2 = 0.6238$, and predicted $R^2 = 0.5252$. The reasonable agreement between adjusted and predicted R^2 values suggests stable predictive capability within the investigated design space. In addition, the low coefficient of variation (1.62 %) and the adequate precision value (11.17) indicate a strong signal-to-noise ratio and good model reliability.

It should be noted that a lack-of-fit test could not be performed because replicate measurements were not retained separately, preventing the decomposition of residual error into pure error and lack-of-fit components. Although this limitation restricts the formal assessment of model inadequacy, the close agreement between adjusted and predicted R^2 values, together with the high adequate precision and low coefficient of variation, indicates that the model does not exhibit significant unexplained systematic deviation within the studied domain.

Table 6. ANOVA of the potable water results

	CSp (potable water), MPa				
	Sum of squares	Degrees of freedom	F-value	p-Value	
Model	451.34	15	5.64	< 0.0001	Significant
A-C	10.44	1	1.96	0.1731	
B-SF/C	4.32	1	0.8096	0.3762	
C-SP/C	0.7229	1	0.1356	0.7156	
D-W/B	2.02	1	0.3794	0.5431	
E-FM	5.04	1	0.9457	0.3395	
AB	24.29	1	4.56	0.0420	
AC	47.39	1	8.89	0.0060	
AD	54.81	1	10.28	0.0034	
AE	60.23	1	11.30	0.0023	
BC	33.62	1	6.31	0.0183	
BD	31.64	1	5.93	0.0217	
BE	14.91	1	2.80	0.1061	
CD	37.93	1	7.11	0.0128	
CE	74.48	1	13.97	0.0009	
DE	49.50	1	9.28	0.0051	
Residual	143.96	27			
Cor total	595.30	42			
	Std. dev.	2.31	R^2	0.7582	
	Mean	142.92	Adj-R^2	0.6238	
	C.V. %	1.62	Pred-R^2	0.5252	
	PRESS	282.64	Adeq Pr	11.1722	

Std. dev: standard of deviation; C.V: coefficient of variation; PRESS: predicted residual error of sum of squares; Adj-R^2: R^2 adjusted; Pred-R^2: predicted R^2; AdeqPr: adequate precision

Model validation is therefore supported by multiple statistical indicators, which consistently confirm its adequacy and predictive performance. This approach is commonly adopted in RSM studies where replicate data are consolidated.

For seawater exposure (Table 7), the quadratic model shows a higher level of statistical significance, with an F-value of 17.47 ($p < 0.0001$), indicating strong model robustness. The model exhibits excellent predictive performance, with $R^2 = 0.9408$, adjusted $R^2 = 0.8869$, and predicted $R^2 = 0.7337$. Several interaction terms, as well as the quadratic effect of cement content, are highly significant, as reflected by their elevated F-values. Although the main effect of cement content remains statistically insignificant when considered independently, its quadratic and interaction contributions become dominant under seawater conditions. This suggests that matrix densification mechanisms play a more direct role in governing compressive strength in aggressive marine environments. To provide a physical interpretation of the statistical results, the significant interaction and quadratic effects identified in the ANOVA can be related to the underlying microstructural behavior of RPC. The interaction between cement content and water-to-binder ratio reflects the degree of matrix densification and particle packing efficiency, which control pore refinement and mechanical strength. Similarly, the interaction between cement content and superplasticizer dosage is associated with improved particle dispersion and matrix homogeneity, while the interaction with fiber volume fraction highlights the balance between matrix strength and crack-bridging mechanisms.

Table 7. ANOVA of the seawater results

	CSs (seawater), MPa				
	Sum of squares	Degrees of freedom	F-value	p-Value	
Model	1735.52	20	17.47	< 0.0001	Significant
A-C	13.53	1	2.72	0.1131	
B-SF/C	0.1520	1	0.0306	0.8627	
C-SP/C	2.48	1	0.4999	0.4870	
D-W/B	0.1803	1	0.0363	0.8507	
E-FM	1.99	1	0.4003	0.5334	
AB	68.97	1	13.88	0.0012	
AC	89.98	1	18.11	0.0003	
AD	57.78	1	11.63	0.0025	
AE	42.78	1	8.61	0.0077	
BC	49.15	1	9.89	0.0047	
BD	75.03	1	15.10	0.0008	
BE	94.53	1	19.03	0.0002	
CD	126.56	1	25.48	< 0.0001	
CE	103.82	1	20.90	0.0001	
DE	140.37	1	28.25	< 0.0001	
A^2	333.71	1	67.17	< 0.0001	
B^2	0.8525	1	0.1716	0.6827	
C^2	0.5166	1	0.1040	0.7501	
D^2	9,52	1	1.92	0.1801	
E^2	3,63	1	0.7306	0.4019	
Residual	109.30	22			
Cor total	1844.82	42			
	Std. dev.	2.23	R^2	0.9408	
	Mean	105.49	Adj-R^2	0.8869	
	C.V. %	2.11	Pred-R^2	0.7337	
	PRESS	491.21	Adeq Pr	17.0088	

Std. dev: standard of deviation; C.V: coefficient of variation; PRESS: predicted residual error of sum of squares; Adj-R^2: R^2 adjusted; Pred-R^2: predicted R^2; AdeqPr: adequate precision

Under seawater exposure, the significant quadratic effect of cement content indicates the existence of an optimal binder content. This behavior results from competing mechanisms: while increasing cement content enhances matrix densification, excessive binder may promote the formation of secondary products such as ettringite and gypsum due to chemical interactions with chloride and sulfate ions. These microstructural changes, supported by XRD and SEM observations, affect pore connectivity and local stress distribution, ultimately influencing compressive strength.

Overall, the ANOVA results demonstrate that compressive strength in RPC is controlled by complex interactions between mixture parameters, with cement content acting as a key interacting factor whose influence depends on both the curing environment and its coupled effects with other variables.

3.2.2. Predictive equations

Based on the ANOVA results, second-order polynomial regression equations were developed to describe compressive

strength in potable water (CSp) and seawater (CSs) as functions of the coded mixture variables. These models are valid within the experimental domain defined in Table 4 and should not be extrapolated beyond the investigated factor ranges.

Potable water:

$$CSp\ (MPa) = 142.92+0.4910A+0.3157B - 0.1292C - 0.2161D - 0.3412E - 0.8713AB - 1.2169AC - 1.3088AD - 1.3719AE + 1.025BC + 0.9943BD + 0.6825BE + 1.0888CD + 1.5256CE = 1.2438DE. \quad (1)$$

Seawater:

$$CSs\ (MPa) = 109.37 + 0.5589A - 0.0592B + 0.2394C + 0.06452D - 0.2143E + 1.4681AB + 1.6769AC + 1.3438A + 1.1563AE - 1.2394ABC - 1.5313BD - 1.7188BE - 1.9888CD - 1.8013CE - 2.0944DE - 3.9468A^2 + 0.1995B^2 + 0.1553C^2 - 0.6667D^2 + 0.4116E^2. \quad (2)$$

3.2.3. Model validation

The predictive capability of the developed RSM models was assessed by comparing experimental and predicted compressive strength values for both curing environments (Fig. 3). For potable water exposure, the predicted and experimental results show a reasonable agreement around the 45° reference line. However, the Predicted R^2 value (0.5252) indicates a moderate predictive capability that should be interpreted with caution, due to the complex and interaction-driven behavior of RPC and the inherent variability of heterogeneous materials.

In this context, the model is better suited for identifying general trends and guiding mixture optimization rather than providing precise point predictions. The observed dispersion is mainly attributed to the combined effects of multiple interacting parameters and microstructural heterogeneities not fully captured by the polynomial model.

Despite this limitation, the agreement between adjusted and predicted R^2 values, along with the adequate precision and low coefficient of variation, confirms that the model remains statistically reliable within the studied domain. For seawater exposure, the model shows improved predictive capability (Predicted $R^2 = 0.7337$), with data more closely clustered around the reference line. This behavior is likely related to the stronger influence of matrix densification mechanisms under marine conditions. In both cases, the high Adequate Precision values confirm a strong signal-to-noise ratio and support the reliability of the models for prediction and optimization.

3.2.4. RSM optimization and response surface analysis

The response surface methodology was employed to analyze the interaction effects between the most influential variables identified by ANOVA and to determine optimal mixture compositions for enhanced compressive strength under both curing conditions. The 3D response surfaces presented in this study illustrate the combined influence of cement content and its significant interacting parameters. In all response surface representations, the remaining variables were maintained at their central coded levels to ensure consistent interpretation of the interaction effects (Fig. 4 and Fig. 5). For potable water curing, the interaction between cement content and water-to-binder ratio clearly demonstrates the importance of matrix densification. Higher cement content combined with lower W/B ratios promotes improved particle packing and reduced porosity, leading to enhanced compressive strength.

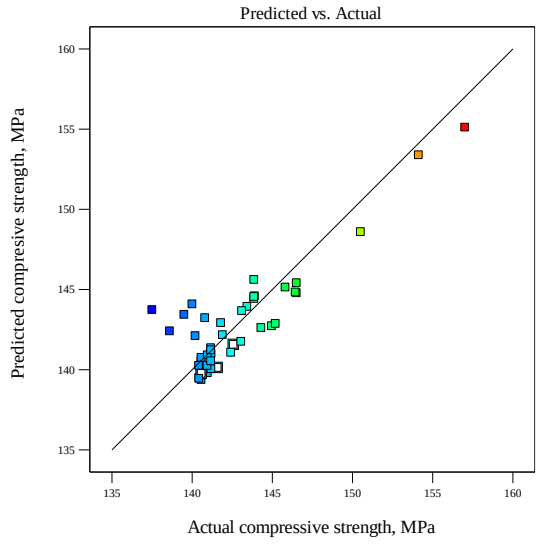

a

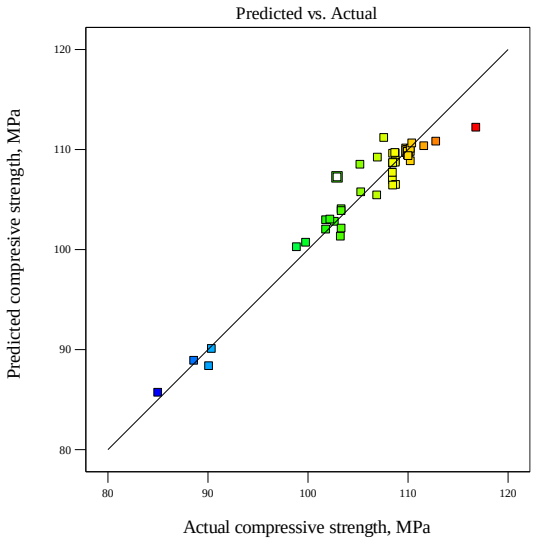

b

Fig. 3. Predicted vs. actual values for the obtained responses: a – Potable water; b – Seawater

The interaction between cement content and fiber volume fraction further highlights the synergistic contribution of matrix strength and crack-bridging mechanisms.

Under seawater exposure, the interaction between cement content and water-to-binder ratio remains the dominant mechanism governing strength performance. A denser microstructure reduces permeability and limits ion ingress, thereby improving resistance to chemical degradation. The interaction between cement content and superplasticizer dosage also plays a relevant role by enhancing dispersion and improving matrix homogeneity.

Optimization results were obtained using a desirability-based numerical approach within the experimental constraints defined by the CCD, confirming that compressive strength maximization is primarily governed

by binder content and matrix compactness. The obtained optimal solutions lie within the investigated experimental domain, ensuring physical consistency and preventing extrapolation beyond validated factor ranges.

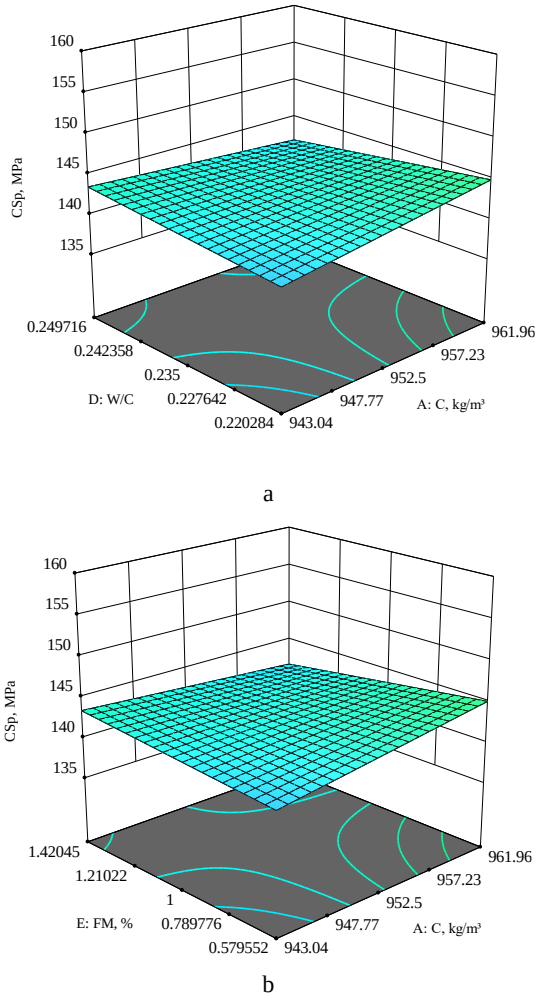

Fig. 4. 3D response surface plots illustrating the combined effects: a – cement content and water-to-binder ratio; b – cement content and fiber volume fraction on the compressive strength of RPC in potable water after 12 months of curing

3.3. Modeling study

The optimized mechanical parameters obtained experimentally through the RSM, particularly the compressive strength in both cases of their immersion in potable water and in seawater, along with the elastic modulus, served as direct input parameters for the Finite Element Method (FEM) and Extended Finite Element Method (X-FEM) simulations. This integration ensured that the numerical modeling accurately reflected the experimental behavior of RPC while also extending the analysis to crack initiation and propagation under realistic structural conditions.

The FEM approach was used to reproduce the mechanical response of RPC specimens under compressive loading, using material parameters directly derived from experimental measurements. The methodology of this approach is consistent with the previous works of Nehar et al. [23, 24], who demonstrated the effectiveness of FEM in characterizing the mechanical behavior of RPC.

To investigate the cracking process, the X-FEM was employed. Unlike conventional FEM, X-FEM enables the modeling of discontinuities, such as cracks, without the need for re-meshing.

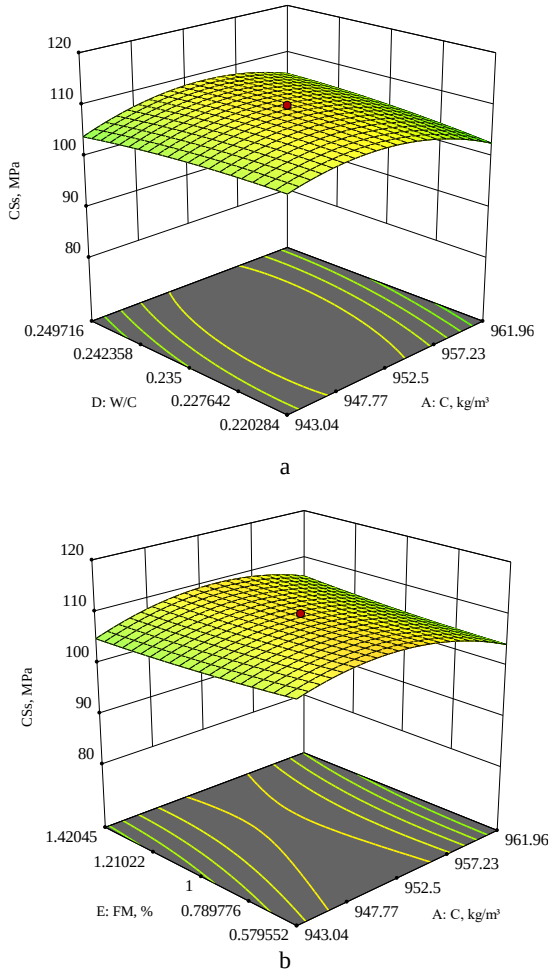

Fig. 5. 3D response surface plots illustrating the combined effects: a – cement content and water-to-binder ratio; b – cement content and superplasticizer dosage on the compressive strength of RPC in seawater after 12 months of curing

This feature is particularly advantageous for simulating the fracture behavior of concrete, where cracks substantially influence global structural integrity. X-FEM introduces additional degrees of freedom near the crack tip, allowing precise tracking of crack propagation. The theoretical background and implementation procedures used in the current study follow the formulations detailed by Nehar et al. [25, 26], who validated this approach for high-performance and fiber-reinforced concretes under different stress conditions.

The RPC samples were modeled as prismatic specimens with dimensions (W, H, ep) = (4, 4, 16) cm³, corresponding to those used in the experimental tests. A quadrilateral mesh was adopted under plane-strain conditions to simulate uniaxial compression, as illustrated in Fig. 6. For crack propagation analysis, a crack of length '*a*' was introduced into the samples to evaluate the stress intensity factors (SIFs) and assess fracture behavior.

The Young's modulus used in the numerical simulations was derived from the experimentally measured

compressive strength according to standard correlations for RPC.

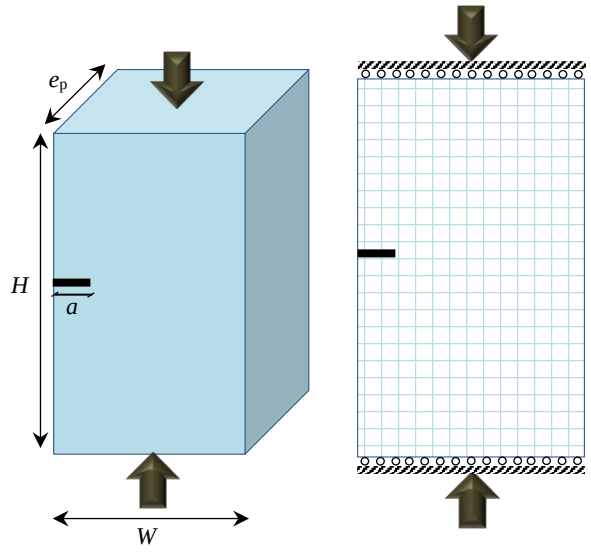

Fig. 6. The modeled RPC samples

Values of 43 GPa and 38 GPa were adopted for specimens cured in potable water and seawater, respectively, while a Poisson's ratio ranging from 0.19 to 0.20 was assumed, in agreement with reported data for ultra-dense cementitious composites.

This combined experimental–numerical framework ensured consistency between measured and simulated responses, providing not only validation of the material parameters but also deeper insights into the structural performance of RPC, especially its crack resistance and long-term durability under marine exposure.

3.3.1. Compressive strength

Fig. 7 presents a comprehensive and detailed comparison of the compressive strengths, which are derived from both experimental data and numerical predictions. This thorough comparison focuses specifically on RPC samples, highlighting the differences between those that contain fibers and those that do not. All of the data is considered under two distinct immersion conditions: one being potable water and the other being seawater. The analysis aims to provide a deeper understanding of how these factors influence the overall compressive strength of the materials.

In potable water (Fig. 7 a), the effect of fiber addition on compressive strength is formulation-dependent rather than systematically beneficial (RPCF1–RPCF3), with a modest gain for RPCF1 (≈ +4 MPa) and RPCF3 (≈ +7 MPa) and a pronounced gain for RPCF2 (≈ +17 MPa), the latter ranking at the upper end of the mixes tested (≈ 157 – 162 MPa, experimental/numerical). The numerical predictions slightly overestimate the experimental values (on the order of 1 – 4 MPa, i.e., < 5 %), indicating overall good agreement of the model. Such deviations remain limited (< 5 %) and can be attributed to the fact that the numerical model idealizes the material as a homogeneous continuum, whereas the experimental behavior is influenced by chemically induced microstructural heterogeneities arising from prolonged marine exposure.

In seawater (Fig. 7 b), a general reduction in the strengths of the RPCF series is observed relative to potable water, and the role of fibers becomes formulation-dependent: they are detrimental for RPCF1 and RPCF2 (decreases of about 8 – 15 MPa), whereas they remain beneficial for RPCF3 (≈ + 10 MPa). Although most mixtures exhibited reduced compressive strength under seawater exposure compared to potable water curing, the reference specimen (RPCC) showed a slightly higher value in this specific dataset.

The numerical predictions show good agreement with the experimental measurements, with deviations generally below 5 %.

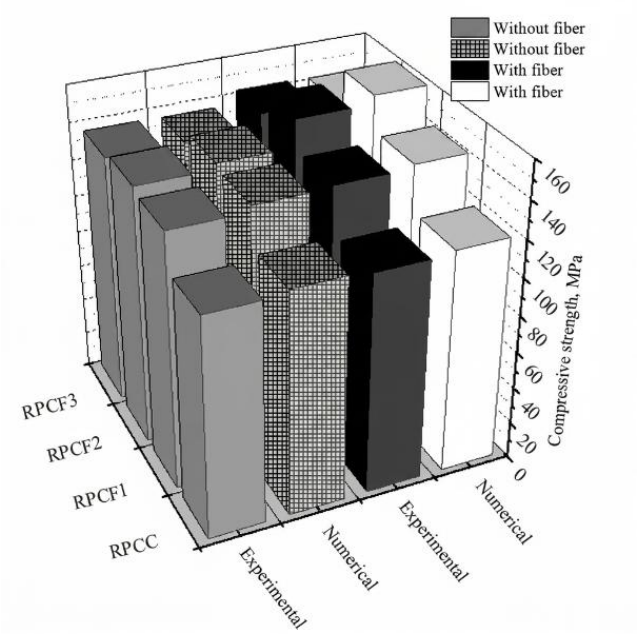

a

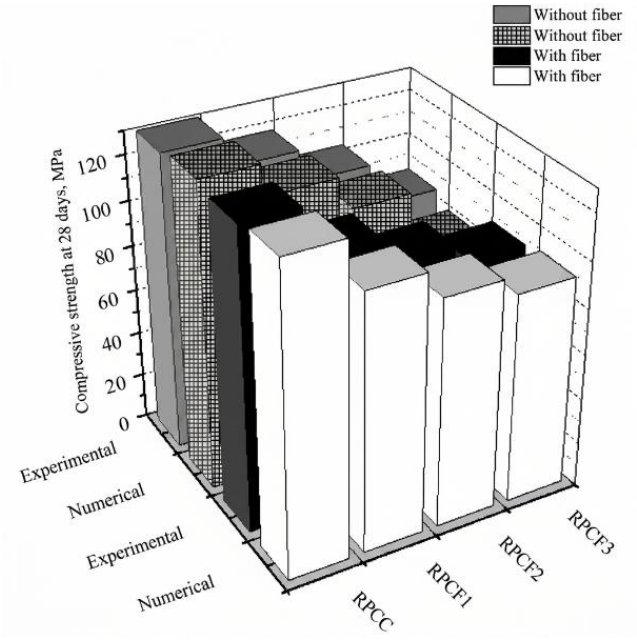

b

Fig. 7. Compressive strength in experimental and numerical cases for RPCF1, RPCF2, and RPCF3 with and without fiber: a – potable water; b – seawater

3.3.2. SIF evaluations

Fig. 8 shows the values of Stress Intensity Factors (SIFs) obtained for RPC samples with cracks.

From a cracking standpoint (Fig. 8), the Mode I stress intensity factor, KI, varies monotonically with the crack-length-to-width ratio (a/W); as a/W increases, the magnitude |KI| also increases, indicating a higher crack-driving force.

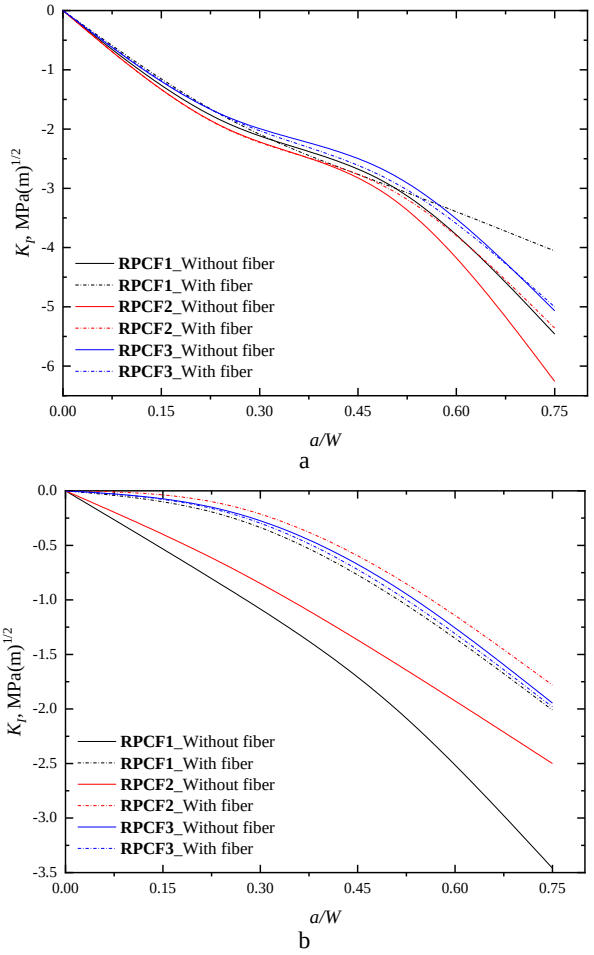

Fig. 8. Mode-I Stress Intensity Factor K_1 versus a/W ratio for RPCF1, RPCF2 and RPCF3 with and without fiber): a – potable water; b – seawater

In potable water (Fig. 8a), the presence of fibers reduces |KI| for all three formulations, signaling an apparent increase in toughness; the effect is noticeable yet moderate, with RPCF2 generally exhibiting the highest |KI| (least tough behavior) and RPCF3 the lowest (most tough).

In seawater (Figure 8b), the fiber-induced reduction in |KI| is more pronounced, especially for RPCF1 and RPCF2 (e.g., at a/W=0.5, |KI| is approximately halved). This suggests that, even though these mixes lose compressive strength in saline conditions, fiber-bridging mechanisms effectively slow crack propagation.

3.4. XRD analysis results

X-ray diffraction (XRD) analysis was used to identify the main crystalline phases formed in the RPC matrix after hydration and long-term exposure to seawater. This analysis is meticulously performed in the well-equipped physics laboratory at the University of Biskra, utilizing a sophisticated X-ray diffractometer (X'Pert) that is intricately coupled with an advanced computer system designed specifically for efficient data processing and analysis.

The diffractograms presented in Fig. 9, Fig. 10, and Fig. 11 reveal the presence of quartz (SiO_2), confirming the incorporation of sand, along with calcite ($CaCO_3$), associated with carbonation processes occurring during hydration and exposure.

Traces of portlandite ($Ca(OH)_2$) were also detected, indicating ongoing hydration reactions. In specimens stored in seawater, the characteristic ettringite peak ($2\theta \approx 50.3°$) appears more pronounced for RPCF1, while the portlandite peak ($2\theta \approx 26.77°$) shows reduced intensity compared to RPCF2. This behavior suggests partial consumption or destabilization of portlandite due to interactions with chloride and sulfate ions present in seawater, leading to the formation of secondary products.

These microstructural changes are consistent with the observed reduction in compressive strength under marine exposure and are in good agreement with previous studies by Chadli et al. [27], Benamara et al. [28], and Yanxia et al. [29], reporting similar phase evolution in aggressive environments.

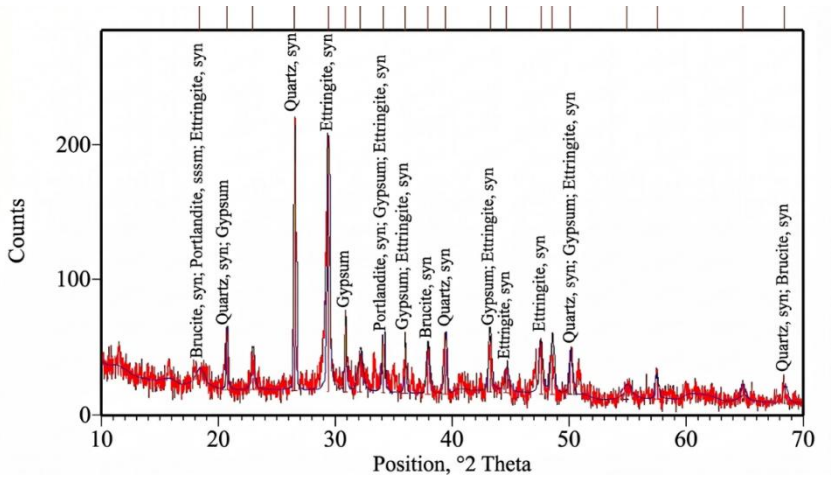

Fig. 9. Diffractogram of fiber-reinforced reactive powder concrete (RPCF) immersed in tap water after 365 days

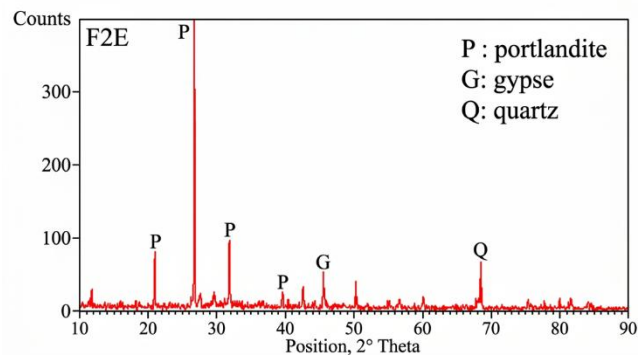

Fig. 10. Diffractogram of RPCF1 stored in seawater, after 365 days

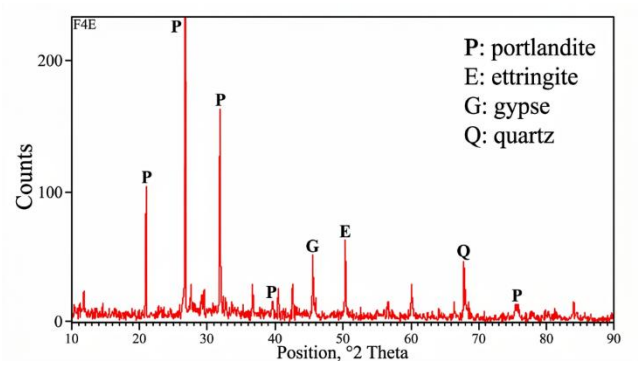

Fig. 11. Diffractogram of RPCF2 stored in seawater, after 365 days

3.5. Scanning electron microscopy results (SEM)

SEM was employed to examine the microstructural features of RPC specimens before and after long-term seawater immersion (Fig. 12: a – graphite spheres embedded in a pearlitic matrix; b – circular cross-section; c – granular and porous surface texture; d – steel fibers; e – steel fibers; f – interfacial adhesion between the cementitious matrix and the steel fibers, and Fig. 13: a – interfacial adhesion between the cementitious matrix and the steel fibers; b – metal fiber vacuum line; c – interaction between fibers and the surrounding matrix; d – pores and fine microstructural defects; e – small cavities formed by material elongation under loading before complete separation; f – gaps and pores). The microstructure is strongly influenced by the binder composition and the formation of pozzolanic reaction products derived from slag and silica fume.

SEM observations indicate that specimens exposed to seawater exhibit a dense and compact matrix characterized by reduced pore size and limited connectivity. This densification is attributed to continued hydration and pozzolanic reactions, which contribute to pore refinement and improved matrix compactness, in agreement with previous observations documented by Chadli et al. [30, 31] and Berkouche et al. [32]. After 365 days, both potable-water- and seawater-exposed specimens display relatively similar overall microstructures, with low porosity and the presence of unreacted slag particles. However, seawater-exposed specimens show higher concentrations of sodium and chloride and localized formation of saline secondary products, likely gypsum.

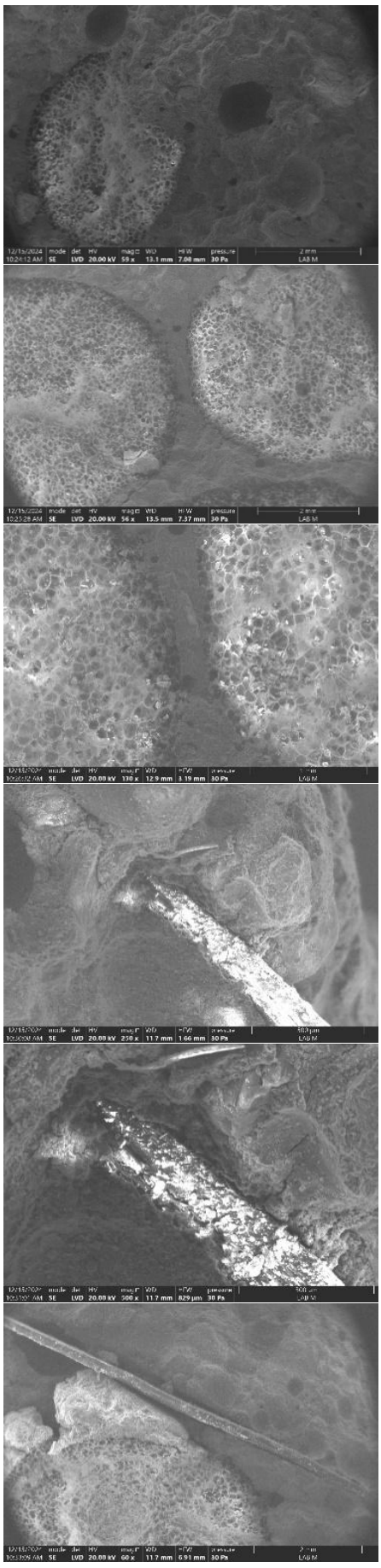

Fig. 12. SEM micrographs of the specimen surface before immersion in seawater

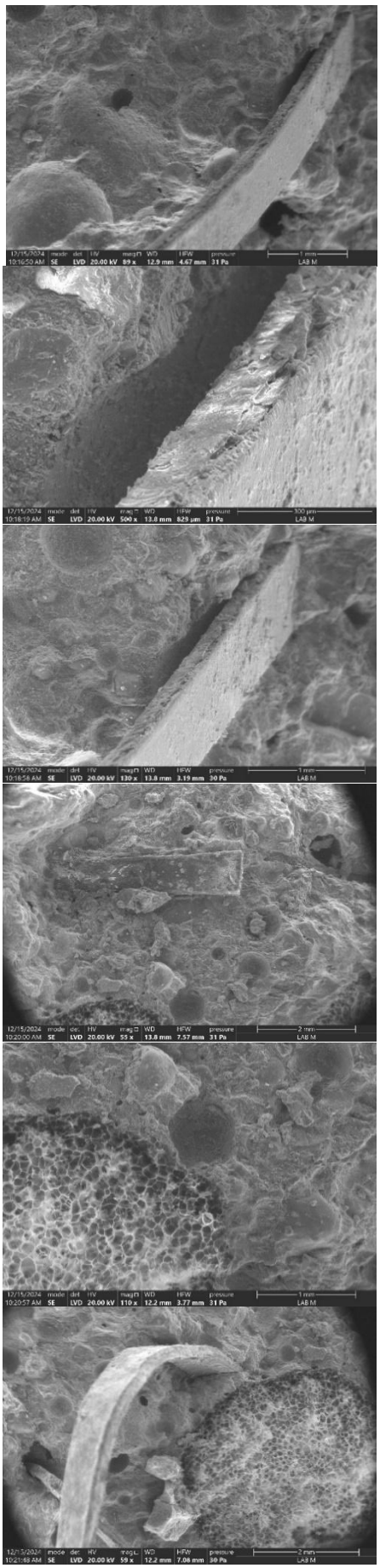

Fig. 13. SEM micrographs of the specimen surface after immersion in seawater

These features provide a microstructural explanation for the slight reduction in mechanical performance observed under marine exposure, as also reported in the literature [33, 34, 35]. No significant cracking or surface degradation was observed in the analyzed micrographs.

4. CONCLUSIONS

This study demonstrates that the long-term performance of RPC under marine exposure is governed by coupled microstructural and mechanical mechanisms that are strongly dependent on mixture composition. The experimental results confirm that seawater alters hydration processes and phase stability, leading to modifications in pore structure and mechanical response that cannot be captured by compressive strength alone.

The statistical analysis based on RSM successfully quantified the individual and interaction effects of key formulation parameters, controlling strength retention in aggressive environments. The high coefficients of determination and predictive accuracy of the developed models demonstrate their suitability as process optimization tools for cementitious material, highlighting the critical role of cement content through interaction and quadratic effects. The difference in predictive performance between potable and seawater models highlights the stronger sensitivity of marine-exposed RPC to matrix densification mechanisms.

Microstructural investigations using XRD and SEM revealed denser matrices and refined pore structures in optimized formulations, despite localized formation of secondary saline products. These observations provide physicochemical explanations for the observed mechanical trends and confirm the critical role of supplementary cementitious materials in enhancing durability.

Numerical simulations using FEM and X-FEM showed strong agreement with experimental results and enabled realistic prediction of crack initiation and propagation. From a fracture mechanics standpoint, fiber incorporation was shown to effectively reduce stress intensity factors and delay crack growth, particularly under marine exposure, even when compressive strength gains were limited.

Overall, the integrated experimental-statistical-numerical framework developed in this work offers a systematic methodology for linking composition, microstructure, and mechanical behavior of RPC under aggressive environments.

REFERENCES

1. **Chadli, M., Mekki, M., Mezghiche, B.** Formulation and Study of Metal Fiber-reinforced Reactive Powder Concrete *World Journal of Engineering* 15 (4) 2018: pp. 531 – 539. https://doi.org/10.1108/WJE-04-2017-0094
2. **Abid, M., Hou, X., Zheng, W., Hussain, R.R.** Effect of Fibers on High-Temperature Mechanical Behavior and Microstructure of Reactive Powder Concrete *Materials* 12 (2) 2019: pp. 329. https://doi.org/10.3390/ma12020329
3. **Yi, Y., Zhu, D., Guo, S., Zhang, Z., Shi, C.** A Review on the Deterioration and Approaches to Enhance the Durability of Concrete in the Marine Environment *Cement and Concrete Composites* 113 2020: pp. 103695. https://doi.org/10.1016/j.cemconcomp.2020.103695

4. **Wang, R., Hu, Z., Li, Y., Wang, K., Zhang, H.** Review on the Deterioration and Approaches to Enhance the Durability of Concrete in the Freeze–Thaw Environment *Construction and Building Materials* 321 2022: pp. 126371. https://doi.org/10.1016/j.conbuildmat.2022.126371
5. **Lafhaj, Z., Dakhli, Z.** Performance Indicators of Printed Construction Materials: A Durability-Based Approach *Buildings* 9 (4) 2019: pp. 97. https://doi.org/10.3390/buildings9040097
6. **Wang, D., Ma, Y., Kang, M., Ju, Y., Zeng, C.** Durability of Reactive Powder Concrete Containing Mineral Admixtures in Seawater Erosion Environment *Construction and Building Materials* 306 2021: pp. 124863. https://doi.org/10.1016/j.conbuildmat.2021.124863
7. **Bertola, F., Gastaldi, D., Canonico, F.** Behavior of Specialty Binders Mixed with Seawater *Advances in Civil Engineering Materials* 8 (2) 2019: pp. 96 – 109. https://doi.org/10.1520/ACEM20180107
8. **Dhondy, T., Remennikov, A., Shiekh, M.N.** Benefits of Using Sea Sand and Seawater in Concrete: A Comprehensive Review *Australian Journal of Structural Engineering* 20 (4) 2019: pp. 280 – 289. https://doi.org/10.1080/13287982.2019.1659213
9. **Cheng, S., Shui, Z., Sun, T., Huang, Y., Liu, K.** Effects of Seawater and Supplementary Cementitious Materials on the Durability and Microstructure of Lightweight Aggregate Concrete *Construction and building Materials* 190 2018: pp. 1081 – 1090. https://doi.org/10.1016/j.conbuildmat.2018.09.178
10. **Sikora, P., Lootens, D., Liard, M., Stephan, D.** The Effects of Seawater and Nanosilica on the Performance of Blended Cements and Composites *Applied Nanoscience* 10 (12) 2020: pp. 5009 – 5026. https://doi.org/10.1007/s13204-020-01328-8
11. **Li, X., Rao, F., Song, S., Ma, Q.** Effect of Cristobalite on the Mechanical Behaviour of Metakaolin-Based Geopolymer in Artificial Seawater *Advances in Applied Ceramics* 119 (1) 2020: pp. 29 – 36. https://doi.org/10.1080/17436753.2019.1687208
12. **Teng, J.G., Xiang, Y., Yu, T., Fang, Z.** Development and Mechanical Behaviour of Ultra-High-Performance Seawater Sea-Sand Concrete *Advances in Structural Engineering* 22 (14) 2019: pp. 3100 – 3120. https://doi.org/10.1177/1369433219858291
13. **Korec, E., Jirásek, M., Wong, H.S., Martínez-Pañeda, E.** A Phase-Field Chemo-Mechanical Model for Corrosion-Induced Cracking in Reinforced Concrete *Construction and Building Materials* 393 2023: pp. 131964. https://doi.org/10.1016/j.conbuildmat.2023.131964
14. **Cui, C., Ma, R., Martínez-Pañeda, E.** A Phase Field Formulation for Dissolution-Driven Stress Corrosion Cracking *Journal of the Mechanics and Physics of Solids* 147 2021: pp. 104254. https://doi.org/10.1016/j.jmps.2020.104254
15. **Zhou, S., Zhuang, X., Rabczuk, T.** Phase-Field Modeling of Fluid-Driven Dynamic Cracking in Porous Media *Computer Methods in Applied Mechanics and Engineering* 350 2019: pp. 169 – 198. https://doi.org/10.1016/j.cma.2019.03.001
16. **NF, P.** "P 18-404: Concrete-Suitability and Control Tests-Manufacture and Curing of Test Specimens." AFNOR, Paris, December 1981.
17. **Belhadj, A., Mahi, A., Derbal, R.** Evaluation of the Durability of Fiber-Reinforced Pozzolanic Concrete in Acidic Environments. 24th French Congress of Mechanics, Brest, 2019, August 26–30.
18. **Chadli, M., Tebbal, N., Mellas, M.** Study of the Mechanical Behavior of a Reactive Powder Concrete Containing Fibers In *International Symposium on Materials and Sustainable Development* 2020: pp. 71 – 82. https://doi.org/10.1007/978-3-030-43211-9
19. **Mounira, C., Rais, S., Ammar, H.** Effect of Dune Sand on the Properties of Reactive Powder Concrete Reinforced with Metal Fibers *Revue des Composites et des Materiaux Avances* 33 (2) 2023: pp. 111. https://doi.org/10.18280/rcma.330206
20. **Nehar, K.C., Benamara, D. Gushgari, S.Y.** RSM-Based Mix Optimization and FEM/X-FEM Crack Modeling of HPSC Elements *Innovative Infrastructure Solutions* 11 (2) 2026: pp. 77. https://doi.org/10.1007/s41062-025-02464-2
21. **Chetbani, Y., Zaitri, R., Tayeh, B.A., Hakeem, I.Y., Dif, F., Kellouche, Y.** Physicomechanical Behavior of High-Performance Concrete Reinforced with Recycled Steel Fibers from Twisted Cables in the Brittle State Experimentation and Statistics *Buildings* 13 (9) 2023: pp. 2290. https://doi.org/10.3390/buildings13092290
22. **Belaadi, A., Boumaaza, M., Alshahrani, H., Bourchak, M.** Effect of Jute Fiber Length on Drilling Performance of Biocomposites: Optimization Comparison between RSM, ANN, and Genetic Algorithm *The International Journal of Advanced Manufacturing Technology* 124 (10) 2023: pp. 3579 – 3599. https://doi.org/10.1007/s00170-022-10801-3
23. **Nehar, K.C., Hachi, B.K., Badaoui, M., Guesmi, M., Benmessaoud, A.** The Evaluation of the spectral Dynamic Stress Intensity Factor by the X-FEM Method Coupled with the Spectral Modal Analysis *Asian Journal of Civil Eng*ineering 17 (6) 2016: pp. 771 – 784.
24. **Nehar, K. C., &Benamara, D.** Experimental Study and Modeling of the Mechanical Behavior of Recycled Aggregates-Based High-Strength Concrete *Fracture and Structural Integrity* 15 (56) 2021: pp. 203 – 216. https://doi.org/10.3221/IGF-ESIS.56.17
25. **Nehar, K.C., Benamara, D., Hamla, W.** Exploitation of Roller Compacted Concrete Based on Recycled Aggregates as a Solution for Degraded Pavements: Experimentation and Modeling *Arabian Journal for Science and Engineering* 47 (4) 2022: pp. 5303 – 5313. https://doi.org/10.1007/s13369-021-06458-x
26. **Nehar, K.C., Benamara, D.** Study of the Structural Behavior of High-Performance Concrete Bridge Decks *International Review of Applied Sciences and Engineering* 16 (1) 2024: pp. 32 – 40. https://doi.org/10.1556/1848.2024.00811
27. **Chadli, M., Bensmail, M., Mellas, M.** Study of the Influence of the Aggressive Environment on the Behavior of Reactive Powder Concrete *Journal of Cement Based Composites* 1 2021: pp. 7 – 12. https://doi.org/10.36937/cebacom.2021.001.002
28. **Benamara, D., Tebbal, N., Rahmouni, Z.E.A.** Durability of High Performance Sandcretes (HPS) in Aggressive Environment *Advances in concrete construction* 8 (3) 2019: pp. 199 – 206. https://doi.org/10.12989/acc.2019.8.3.199
29. **Cai, Y., Lin, Z., Zhang, J., Lu, K., Wang, L., Zhao, Y., & Huang, Q.** Dosage Effect of Wet-Process Tuff Silt Powder as an Alternative Material of Sand on the Performance of Reactive Powder Concrete *Materials* 15(11) 2022: pp. 3930.

https://doi.org/10.3390/ma15113930

30. **Chadli, M., Almeasar, K.S., Rais, S., Mellas, M., Hamlaoui, A.** Exploring the Potential of Waste Marble Powder and Metal Fibers for Enhancing Reactive Powder Concrete Performance at Elevated Temperatures *Innovative Infrastructure Solutions* 10 (4) 2025: pp. 1 – 14. https://doi.org/10.1007/s41062-025-01940-z
31. **Chadli, M., Tebbal, N., Mellas, M.** Impact of Elevated Temperatures on the Behavior and Microstructure of Reactive Powder Concrete *Construction and Building Materials* 300 2021: pp. 124031. https://doi.org/10.1016/j.conbuildmat.2021.124031
32. **Berkouche, A., Belkadi, A.A., Hasnaoui, A., Aggoun, S., Chiker, T., Khechai, A., Tayebi, T.** Enhancing Sustainable Construction Practices: Utilizing Heat-Treated Recycled Concrete Fines for Improving Slag-Based Geopolymer Materials *Arabian Journal for Science and Engineering* 50 (16) 2025: pp. 12717 – 12734. https://doi.org/10.1007/s13369-024-09477-6
33. **Kim, S., Usman, M., Park, C., Hanif, A.** Durability of Slag Waste Incorporated Steel Fiber-Reinforced Concrete in Marine Environment *Journal of Building Engineering* 33 2021: pp. 101641. https://doi.org/10.1016/j.jobe.2020.101641
34. **Calvo, J.G., Alonso, M.C., Luco, L.F., Velasco, M.R.** Durability Performance of Sustainable Self Compacting Concretes in Precast Products Due to Heat Curing *Construction and Building Materials* 111 2016: pp. 379 – 385. https://doi.org/10.1016/j.conbuildmat.2016.02.097